Meso–Macro Energy Exchange in Shock-Wave Processes and Dynamic Strength of AB2 Steel

Yu. I. Meshcheryakov[1]*, G. V. Konovalov[1], N. I. Zhigacheva[1], and A. K. Divakov[1]

[1] *Institute for Problems in Mechanical Engineering, Russian Academy of Sciences, Saint Petersburg, 199178 Russia*
* e-mail: ym38@mail.ru

Abstract—Impact tests of low-alloy martensitic-bainitic steel AB2 showed that the scale of dynamic deformation and the fracture mechanism change in a threshold manner. The change in the mechanism and scale of fracture is triggered by the resonant excitation of large-scale structural elements of the material (grain conglomerates) due to plastic flow oscillations. In this case, the grain-boundary mechanism of dynamic fracture is replaced by a transcrystalline one. Beyond the strain rate threshold, mesoscopic elementary carriers of dynamic deformation are divided into two groups: low-velocity and high-velocity. Accordingly, the velocity distribution of mesoparticles shows two humps. The velocity spread of mesoparticles sharply increases under these conditions, while the mass velocity defect (change in the shock wave amplitude) becomes negative. The latter fact indicates the local acceleration of mesoparticles in discrete regions of the target (the so-called shooting of mesoparticles in the shock wave direction). Transcrystalline cracks are randomly distributed throughout the specimen and have a random orientation.

Keywords: multiscale deformation, velocity variation, velocity defect, spall strength, trigger mechanism

DOI: 10.1134/S1029959924010107

1. INTRODUCTION

Experimental studies of high-speed processes in condensed matter face not only technical difficulties associated with measurements on small spatiotemporal scales but also fundamental difficulties in processing and interpreting the derived data. If the size of the averaging region becomes commensurate with the size of a structural element of the medium, the measured value no longer refers to the macroscopic scale. In the case of dynamic processes, it is most often an intermediate scale between the micro- and macroscales, which corresponds to the scale of the internal structure of the medium [1–5].

Experiments proved that the common assumption on the conversion of 90–95% of the plastic work to heat was invalid under dynamic deformation [6]. The authors of [6] measured a fraction of the plastic work converted to heat during impact loading of the 2023-T3 aluminum alloy and α titanium. It was found that only 35–50% of the work of dynamic deformation is converted to heat. The rest energy is stored in the material as latent energy in the form of structural defects, cracks, localized shear bands, and other structural imperfections.

2. EXPERIMENTAL PROCEDURE

We run impact tests under uniaxial strain conditions (plate impact). Impact loading of AB2 steel targets 52 mm in diameter and 5 mm in thickness is performed using a 37 mm single-stage light gas gun. Impactors present cups 28 mm in diameter with the bottom thickness 2 mm made of high-strength tool steel U8 (RC 64). The procedure of impact loading with the light gas gun (working on helium) and measurement of the target response was described in [7]. The experimental setup and impactor are schematized in Figs. 1 and 2, respectively. The principle of interferometry and recording of free surface velocity profiles was detailed in [8–10]. In the present tests, the impact velocity is determined by measuring the time the impactor flights between two laser beams (Fig. 1). The mass velocity defect (a decrease in the signal amplitude on the compression pulse plateau) is determined based on the independent measurement of the free surface velocity U_{fs} and the impact velocity. As is known, at symmetrical collision, the mass velocity U_p is half the impact velocity, i.e. $U_p = 0.5U_{imp}$. On the other hand, when the wave arrives at the free surface, the mass velocity doubles, i.e. $U_{fs} = 2U_p$,
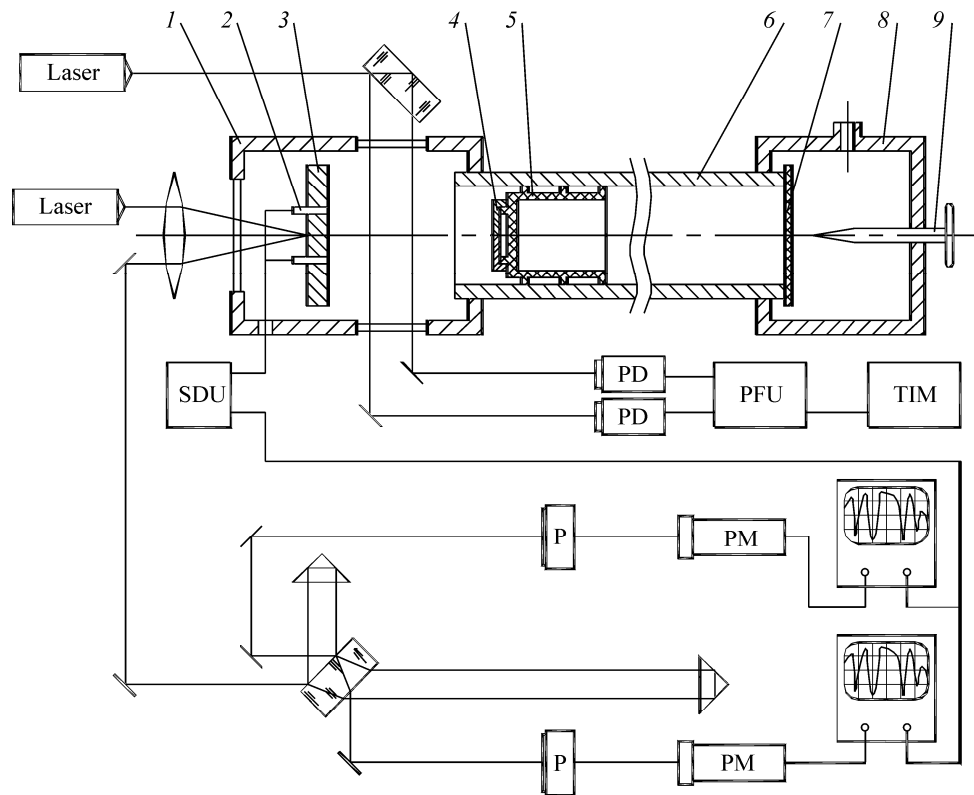
Fig. 1. Experimental setup and measuring circuit: vacuum chamber (*1*); pins (*2*); target (*3*); impactor (*4*); sabot (*5*); barrel (*6*); membrane (*7*); high pressure chamber (*8*); membrane penetration device (*9*); PD—photodetectors; PFU—pulse forming unit; TIM—time interval meter; P—polaroid; SDU—signal delay unit; PM—photomultiplier.

whence it follows that $U_{imp} = U_{fs}$ upon zero momentum loss. However, this relation does not hold in reality because the target material loses momentum due to internal processes of structural heterogenization. In this case, the velocity defect is defined as the difference between the impact velocity and the maximum free surface velocity on the compression pulse plateau.
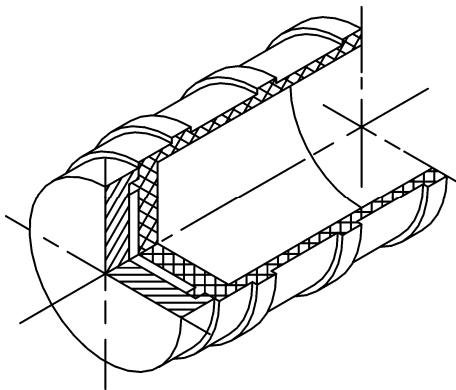

Fig. 2. Impactor with the sabot.

The aim of the present work is to clarify the following questions of the physics of multiscale dynamic deformation and fracture: how momentum and energy is exchanged between scales, and what triggers the transition of dynamic fracture from one scale to another. Answers to these questions are found by considering the problem of shock wave propagation in a heterogeneous relaxing medium, running impact tests on AB2 steel with the measurement of the material response parameters on two scales, and performing microstructural studies of steel specimens loaded below, at, and above the impact velocity threshold.

The velocity defect is a macroscopic quantity that characterizes the change in the average mass velocity due to the exchange of momentum between the meso- and macroscales. As the diameter of the probing laser beam of the interferometer does not exceed 50–70 μm, the recorded impact response corresponds to the response of a large-scale structural element, which is classified as the meso-2 scale according to [1].

The impact tests on AB2 steel specimens reveal two characteristics of multiscale dynamic deforma-
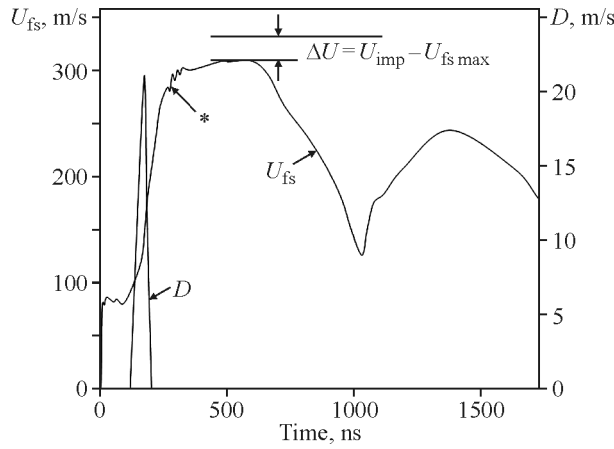
Fig. 3. Time profiles of the free surface velocity U_{fs} and velocity variation D in a 5-mm-thick target made of AB2 steel at the impact velocity 324 m/s. The asterisk * indicates plastic flow oscillations in transition to the pulse plateau.

tion and fracture: there is a certain threshold strain rate, at which the impact response characteristics change sharply, namely, mass velocity variation D and the velocity defect on the compression pulse plateau ΔU. These characteristics are illustrated in Fig. 3 by the free surface velocity profile recorded during impact loading of the AB2 steel target under uniaxial deformation at the impact velocity 324 m/s. Results of testing AB2 steel in the impact velocity range 125–455 m/s are given in Table 1. Figure 4 plots the dependences of the velocity variation $D = f(U_{imp})$ and the velocity defect $\Delta U = f(U_{imp})$ on the impact velocity.

Table 1. Velocity defect, velocity variation, and spall strength of AB2 steel at different impact velocities

U_{imp}, m/s	ΔU, m/s	D, m/s	W, m/s
125	7.2	0.0	131.0
149	9.8	0.0	140.0
185	21.2	0.0	146.0
241	−1.2	0.0	172.0
285	10.0	0.0	175.0
324	2.5	0.0	174.0
361	39.4	21.0	159.0
381	9.1	0.0	190.0
402	25.7	29.0	170.0
432	−50.0	35.0	198.0
441	−50.0	42.8	196.3
455	−26.9	–	202.0

As can be seen from Fig. 4, starting from the impact velocity 381 m/s, the rate of change of the velocity variation dD/dt reverses sign, and D itself increases sharply. At the same time, the velocity defect becomes negative. A negative value of the velocity defect means that, instead of the compression pulse attenuation, there is an acceleration of local meso-2 regions of the target material in the direction of wave propagation. To find out the mechanism of formation of the negative velocity defect, we address time profiles of the free surface velocity recorded below (impact velocity 324 m/s, Fig. 5a) and above the strain rate threshold (impact velocity 432 m/s, Fig. 5b). Let us further use the relation between the mass velocity variation in the loading wave on the mesoscale, D, and the strain rate $d\varepsilon/dt$ [11, 12]:

$$D = R\frac{d\varepsilon}{dt}. \qquad (1)$$

Under uniaxial impact loading, the strain rate is related to the mass velocity in the loading wave as follows:

$$\frac{d\varepsilon}{dt} = \frac{1}{C_p}\frac{du}{dt}. \qquad (2)$$

By differentiating the mass velocity-time profiles (Figs. 5a, 5b) and using relations (1) and (2), the time profile of the velocity variation $D(t)$ can be plotted. In the case of AB2 steel, this gives two different dependences $D(t)$. Figure 6 shows the results of differentiating two time profiles of the free surface velocity recorded at the impact velocities 324 m/s (below the threshold, Fig. 6a) and 432 m/s (above the threshold, Fig. 6b). It is seen that the behavior of the velocity variation below the impact velocity threshold differs sharply from that above the threshold. The
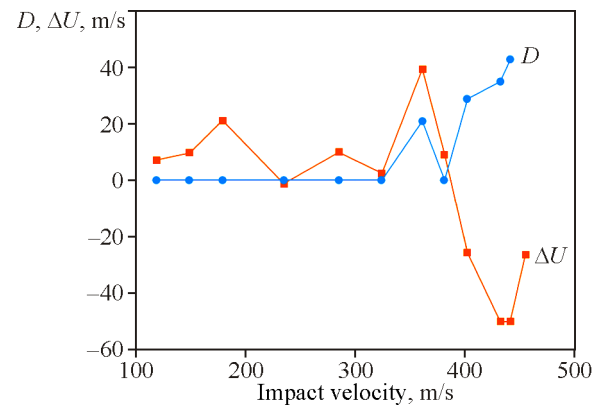

Fig. 4. Velocity variation D and velocity defect ΔU as a function of the impact velocity at symmetrical collision with AB2 steel (color online).
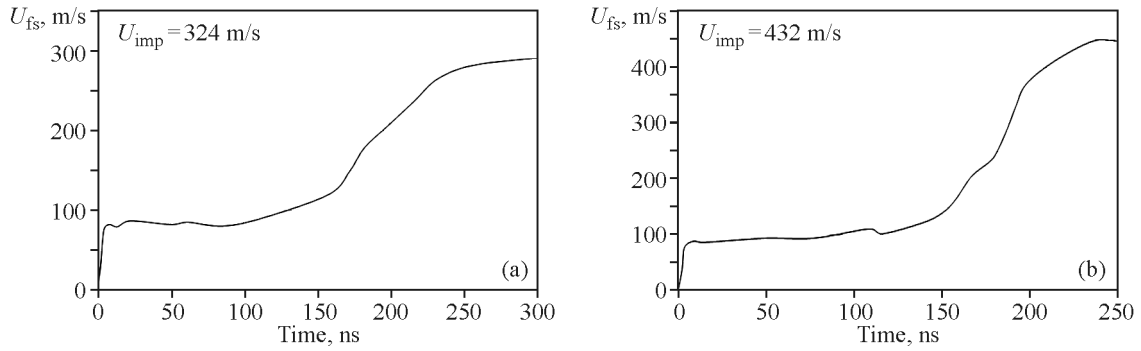
Fig. 5. Time profiles of the free surface velocity in AB2 steel at the impact velocities 324 (a) and 432 m/s (b).

mesoscopic velocity variation curve has one hump in the prethreshold region, while it has two humps in the postthreshold region. Consequently, particles are also differently grouped depending on the strain rate. From microstructural studies (described below) of specimens loaded in different impact velocity regions, it is clear that different curves below and above the impact velocity threshold correspond to different structural elements. From the velocity variation curves in the postthreshold region (Fig. 6b) it follows that the second group of particles falls behind the first group by 27.5 ns.

This raises the question of what trigger mechanisms are responsible for the transition of a dynamically deformed material from one scale to another. The high time resolution methods (0.6–1.0 ns) used in the tests allow detecting plastic flow oscillations. It is found that the period of oscillations depends on the strain rate. Figure 7 shows the velocity-time pro-

file of the specimen free surface at the impact velocity 361 m/s.

The presented free surface velocity profile reveals oscillations with the period ≈11 ns. Comparison of the oscillation periods recorded using the high-speed interferometer with the oscillation parameters calculated by the relaxation model of the medium dynamics and with the microstructural results for AB2 steel specimens will be made below.

3. TRIGGER MECHANISMS OF THE DYNAMIC FRACTURE SCALE CHANGE

As theoretical and experimental studies show, one of the characteristic features of dynamic deformation is mass velocity oscillations. The process of excitation of short-lived mass velocity oscillations during dynamic deformation was theoretically investigated in [11, 12]. These mass velocity oscillations are caus-
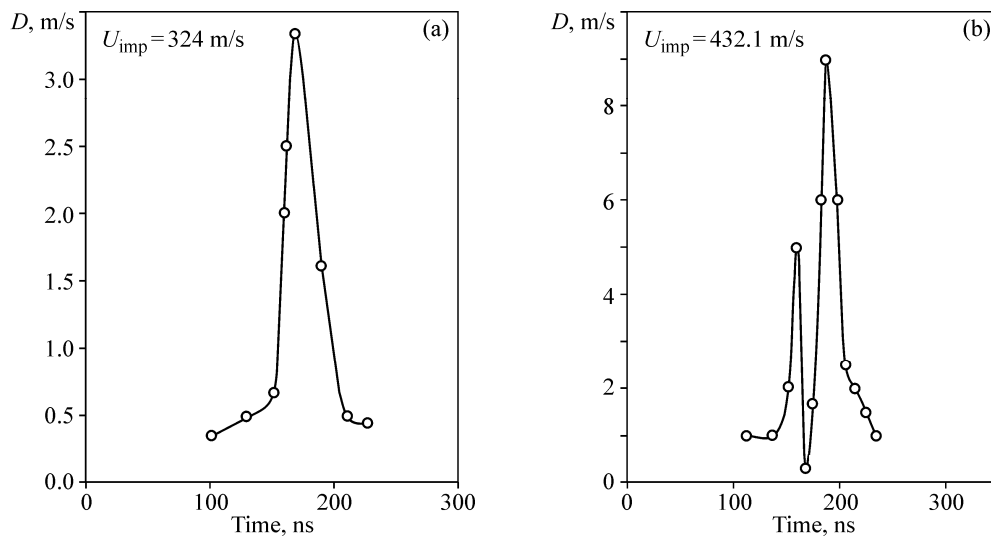

Fig. 6. Time profiles of velocity variation D below (a) and above the impact velocity threshold (b).
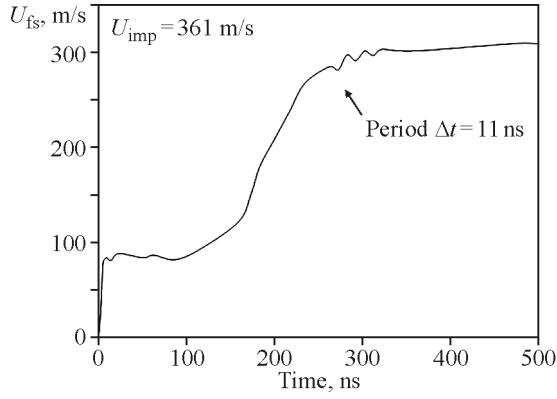
Fig. 7. Time profile of the free surface velocity U_{fs} of AB2 steel at the impact velocity $U_{imp} = 361$ m/s.

ed by sign polarization of the dislocation structure in random stress fields. This results in the formation of mesoparticles, which present dislocation groups of the same sign and have the lifetime between 150–200 ns. In this case, the process of wave front propagation in a heterogeneous medium can be treated as the superposition of two modes: propagation of the plane wave front (mode 1), and random propagation of individual volumes of the medium (mesoparticles) under the influence of random fields of internal stresses (mode 2). Representing dynamic deformation as additive propagation modes significantly simplifies the description of the shock wave process in the heterogeneous medium and allows employing statistical moments of the mesoparticle velocity distribution function $f(v, r, t)$. Under nonuniform dynamic deformation, the zero statistical moment of the function is the mesoparticle density $\rho(r, t)$, the first moment is the average mesoparticle velocity $u(r, t)$, and the second moment is the mesoparticle velocity dispersion $D^2(r, t)$:

$$\rho(r, t) = \int_{-\infty}^{\infty} f(r, v, t) \mathrm{d}v,$$

$$\bar{u}(x, t) = \frac{\int_{-\infty}^{\infty} v f(x, v, t) \mathrm{d}v}{\rho}, \qquad (3)$$

$$D^2 = \int_{-\infty}^{\infty} (v - \bar{u})^2 f(x, v, t) \mathrm{d}v.$$

In shock wave processes, the time required for the particle velocity distribution function to become equilibrium is very short compared to the duration of the shock wave front. Numerical modeling of shock wave propagation in copper showed that the velocity

distribution function became equilibrium within 11.5 ns [13]. This justifies the reduction of the analysis from the whole distribution function to two statistical moments of the function, namely, mathematical expectation (the average particle velocity in the loading wave) and mass velocity dispersion. The interferometric method used in the tests for recording the shock wave process allows measuring these two characteristics in real time.

The correlated behavior of the dependences of velocity variation $D = f(U_{imp})$ and velocity defect $\Delta U = f(U_{imp})$ suggests that they are interrelated in a certain way. The recorded response of the material to impact loading reveals that the mass velocity variation increases sharply starting from the impact velocity 381 m/s. This points to the excitation of mass velocity oscillations in the impact velocity range 361–381 m/s. In addition, starting from the impact velocity 381 m/s, the velocity defect on the compression pulse plateau becomes negative. To explain these unusual and important phenomena, the shock wave process is modeled within the relaxation model of a dynamically deformed medium and microstructural evolution of the material is thoroughly studied at different stages of shock wave loading.

The representation of the mesostructure as a set of one-sign dislocation groups formed due to the dislocation structure polarization [5, 11, 12] revealed an analytical connection between the mass velocity defect and velocity dispersion on the mesoscale. The velocity defect is determined by the behavior of the velocity variation on the meso-2 scale. It was shown that the mass velocity defect and velocity dispersion were not independent quantities [14, 15]:

$$\Delta U = \pm \frac{1}{2} \frac{\mathrm{d}D^2}{\mathrm{d}u}. \qquad (4)$$

Relations (4) can be written as follows:

$$\Delta U = \pm D \frac{\mathrm{d}D/\mathrm{d}t}{\mathrm{d}u/\mathrm{d}t}. \qquad (5)$$

The sign $\pm$ in expressions (4) and (5) means that, depending on the sign of the derivative $\mathrm{d}D/\mathrm{d}t$, the mass velocity defect decreases due to dispersion variation or increases. Using relations (1) and (2), the mass velocity defect can be expressed through the rate of change of mass velocity variation in the following form:

$$\Delta U = \pm \frac{R}{C_p} \frac{\partial D}{\partial t}. \qquad (6)$$

From Eqs. (1) and (2), passing to strain according to (2), we derive

$$\Delta U = \pm \frac{R^2}{C_\mathrm{p}} \frac{\partial^2 \varepsilon}{\partial t^2}. \qquad (7)$$

For the impact response of a relaxing heterogeneous medium, relations (1) and (6) are used to construct a constitutive equation that closes the balance equations. In the case of one-dimensional shock wave propagation, the momentum balance equation and the continuity equation have the following forms:

$$\rho \frac{\partial u}{\partial t} - \frac{\partial \sigma}{\partial x} = 0, \qquad (8)$$

$$\frac{\partial u}{\partial x} - \frac{\partial \varepsilon}{\partial t} = 0. \qquad (9)$$

Balance Eqs. (8) and (9) can be reduced to the second-order differential equation

$$\rho \frac{\partial^2 \varepsilon}{\partial t^2} - \frac{\partial^2 \sigma}{\partial x^2} = 0. \qquad (10)$$

In [16, 17], balance Eqs. (8) and (9) are closed using the relaxation constitutive equation

$$\sigma - \rho C_l^2 \varepsilon = -2\mu \varepsilon^\mathrm{p}, \qquad (11)$$

or the differential one

$$\frac{\partial \sigma}{\partial t} - \rho C_l^2 \frac{\partial \varepsilon}{\partial t} = -2\mu \frac{\partial \varepsilon^\mathrm{p}}{\partial t}. \qquad (12)$$

Here ε is the total (elastic + plastic) strain in the wave direction, ε^p is the plastic strain, μ is the shear modulus, C_l is the longitudinal sound velocity, and C_p is the plastic wave velocity. The relaxation function

$$F = 2\mu \frac{\partial \varepsilon_\mathrm{p}}{\partial t} \qquad (13)$$

is expressed through the well-known Orowan equation

$$\frac{\partial \varepsilon_\mathrm{p}}{\partial t} = b N_\mathrm{d} V_\mathrm{d}, \qquad (14)$$

where the macroscopic plastic strain rate $d\varepsilon^\mathrm{p}/dt$ is determined by the density N_d and velocity V_d of mobile dislocations. This approach assumes additive contributions of dislocations to the total strain rate. It was found that the study of shock wave processes in a solid with consideration for only additive relaxation mechanisms provided inadequate description not only of the plastic front of an elastoplastic wave but even of the elastic precursor attenuation [18–22]. These facts became the main reason for including the mesoscale in the description of dynamic deformation processes. The inclusion of the mesoscale in the description of shock wave processes was justified in [23] within the statistical mechanics of nonequilibrium processes.

Regardless of what physical mechanisms and elementary carriers of deformation on the atom-dislocation scale provide relaxation of internal stresses (dislocations, point defects, phase transformations, localized shear, rotations, etc.), the relaxation of the material under impact loading results in the velocity defect $\Delta U \neq 0$. Within this approach, the constitutive equation to close balance Eqs. (8) and (9) can be written in the following form:

$$\frac{\partial \sigma}{\partial t} - \rho C_l^2 \frac{\partial \varepsilon}{\partial t} = \frac{2\mu}{C_\mathrm{p}} \frac{\partial (\Delta U)}{\partial t}. \qquad (15)$$

In this constitutive equation, the role of the relaxation function is played by the right side of the equation. The advantage of this approach is that the relaxation model does not include dislocation parameters, such as the average density N_d and velocity V_d, which cannot be controlled under dynamic deformation of the material. Unlike the dislocation structure parameters, the mass velocity defect is a quantity measured in real time. Double differentiation of Eq. (11) with respect to the x coordinate and substitution of $\partial^2 \sigma / \partial x^2$ from Eq. (10) give

$$\rho C_\mathrm{p}^2 \frac{\partial^2 \varepsilon}{\partial t^2} - \rho C_l^2 \frac{\partial^2 \varepsilon}{\partial x^2} = -2\mu R^2 \frac{\partial^2 \Delta U}{\partial x^2}. \qquad (16)$$

Using (7), we have

$$\rho C_\mathrm{p}^2 \frac{\partial^2 \varepsilon}{\partial t^2} - \rho C_l^2 \frac{\partial^2 \varepsilon}{\partial x^2} + 2\mu R^2 \frac{\partial^4 \varepsilon}{\partial x^2 \partial t^2} = 0. \qquad (17)$$

In the tests, we have a stationary plastic wave front. As shown in [24, 25], in the case of the stationary plastic front, the maximum velocity-time variation $D_{\max}$ coincides with the middle of the plastic front, where the strain rate is also maximum. As can be seen from Fig. 3, the same occurs during impact loading of AB2 steel targets. In this case, a transition to one independent variable $\varsigma = x - C_\mathrm{p} t$ is possible. Equation (15) takes the form

$$\rho (C_l^2 - C_\mathrm{p}^2) \frac{\partial^2 \varepsilon}{\partial \varsigma^2} + 2\mu R^2 \frac{\partial^4 \varepsilon}{\partial \varsigma^4} = 0. \qquad (18)$$

After replacing $\varepsilon_{\varsigma\varsigma} = \psi$, we obtain the oscillator equation

$$\rho (C_l^2 - C_\mathrm{p}^2) \psi + 2\mu R^2 \psi_{\varsigma\varsigma} = 0, \qquad (19)$$

or

$$\psi_{\varsigma\varsigma} + k^2 \psi = 0. \qquad (20)$$

From Eq. (20) follows

$$k^2 = \frac{\rho (C_l^2 - C_\mathrm{p}^2)}{2\mu R^2}. \qquad (21)$$

The wave vector and consequently the spatial period of oscillations $\lambda = 2\pi/k$ are seen to depend on the

plastic front velocity. In the tests, the plastic wave velocity in AB2 steel is determined to be $C_p = 4.6 \times 10^5$ cm/s at the impact velocity 361 m/s. The time profile of the mass velocity corresponds to the strain rate at the plastic wave front $d\varepsilon/dt = 2.02 \times 10^6$ s^{-1} and the mass velocity variation $D = 21$ m/s (Table 1, Fig. 3). Then, from relation (1), $R = 1.002 \times 10^{-3}$ cm. From (21), $k = 0.785 \times 10^3$ cm^{-1}. In this case, the spatial period of oscillations is equal to $\lambda = 2\pi/k = 53.22$ μm, which corresponds to the time period $T = 10.28$ ns. The calculated oscillation period almost coincides with the experimentally recorded one $T \approx 11$ ns (Fig. 7). This makes the resonant interaction between structural elements of the medium and oscillations of the plastic front possible in this strain rate range. This coincidence is a prerequisite for the excitation of mesoscopic structural elements, leading to a change in the mechanism of dynamic fracture of the material. The resonant excitation of structural elements of the material is the first mechanism triggering the change of scale and mechanism of dynamic fracture of AB2 steel.

The second trigger mechanism that changes the shock wave behavior of AB2 steel is the sign reversal of the velocity defect. In expression (4), the sign of the velocity defect ΔU is determined by changes in the velocity variation dD/dt. Thus, if the velocity variation of mesoparticles first decreases and then increase during dynamic deformation, the velocity defect changes sign. Consequently, the sign of Eq. (19) also reverses. This makes the solution to Eq. (19) unstable: it describes the unlimited growth of plastic flow rather than oscillations. The microstructural studies point to a highly developed plastic flow in the impact velocity range 324–361 m/s, causing a reduction of grain conglomerates from 80–100 to 50–60 μm. In addition, resonant excitation of grain conglomerates at the impact velocity 361 m/s leads to further refinement. These processes cause the velocity variation to abruptly increase. In the impact velocity range 361–381 m/s, the velocity variation drops from 21 m/s to zero, and, at the impact velocity 381 m/s, it increases again. At this impact velocity, the derivative dD/dt reverses sign, and the mass velocity defect becomes negative according to expression (4).

The transfer of energy from the macro to meso-2 scale can be easily estimated knowing the mass velocity defect. In the paper, energy exchange is estimated for a meso-2 element 100 μm in size, which corresponds to the diameter of the laser beam of the interferometer used to record the velocity defect equal to

Table 2. Results of calculation of local meso–macro energy exchange

U_{imp}, m/s	ΔU, m/s	L, μm	E, erg
125	7.2	100.0	2.040
149	9.8	100.0	3.770
185	21.2	0.0	17.640
241	−1.2	0.0	0.052
285	10.0	0.0	3.925
324	2.5	0.0	0.245
361	39.4	21.0	60.900
381	9.1	0.0	3.250
402	25.7	29.0	25.940
432	−50.0	35.0	98.250
441	−50.0	42.8	98.250
455	−26.9	–	28.400

$\Delta U = 25$ m/s. The calculation results for meso–macro energy exchange are given in Table 2.

Figure 8 shows the dependence of the energy transferred from the macroscale to a meso-2 element. It can be seen that the transferred energy increases sharply after the impact velocity 381 m/s.

4. SPALL STRENGTH

One of the most important characteristics of a structural material operating under impact loading is spall strength. In the test, the spall strength in the form of the so-called "pull-back velocity" is determined from the time profiles of the free surface velocity by the well-known method [26] as the difference between the maximum free surface velocity and the
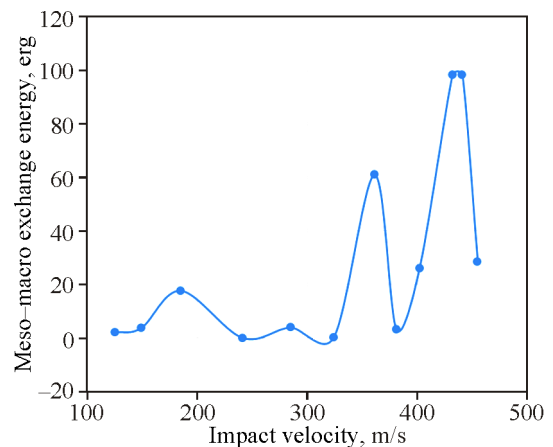

Fig. 8. Dependence of the energy transferred from the macroscale to a meso-2 element on the impact velocity.
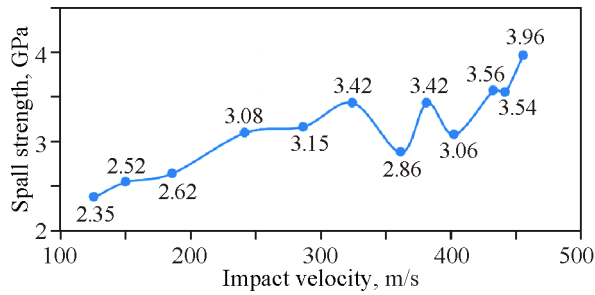
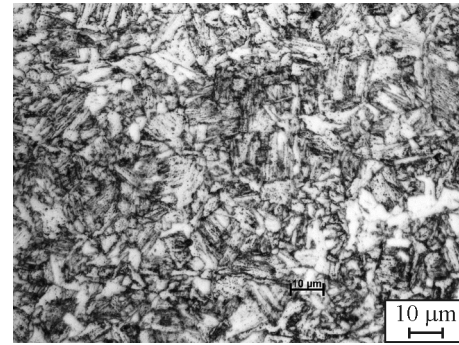**Fig. 9.** Dependence of spall strength of AB2 steel on the impact velocity.

Fig. 10. Initial microstructure of AB2 steel.

first minimum velocity on the trailing edge of the compression pulse (here, spall strength is expressed in GPa). In the impact velocity range 381–441 m/s, the spread of spall strength values is seen to increase. This behavior is related to a change in the pattern of dynamic fracture. Since the diameter of the laser beam of the interferometer used to record the impact response of the target material does not exceed 50–70 μm, the spall strength corresponds to the local dynamic strength of a meso-2 element. Due to the mass velocity scatter at different points of the target, the local spall strength also experiences a certain scatter. This scatter begins at the impact velocity above the threshold 381 m/s and correlates with the behavior of the velocity variation and velocity defect. Starting from the impact velocity 381 m/s, the average spall strength increases, although the spread of its values also increases. At the resonant velocity 361 m/s, the spall strength has a local minimum ($W = 2.86$ GPa) (Fig. 9). This indicates that, when resonant with a shock wave, the material softens.

5. MICROSTRUCTURAL STUDIES

Further identification of the mechanisms of change of the impact fracture scale was carried out under microstructural studies of specimens made of fine-grained martensitic-bainitic steel AB2 (220 NV) with the maximum grain size 15 μm (Fig. 10). The chemical composition of AB2 steel is presented in Table 3.

For microstructural studies, the test specimens were cut along one of the planes in the impact direction, polished, etched in the 5% nitric acid solution,

and then examined under an Axio Observer Z1m microscope. The studies show that, at the impact velocity ~361 m/s, the fracture mechanism changes from grain-boundary to transcrystalline. Based on the modeling results given in Sect. 3, this transition can be explained by the excitation of plastic flow oscillations at a certain strain rate, when the period of oscillations coincides with the average size of the structural element.

At the impact velocity 324 m/s, plastic flow is most pronounced (Figs. 11c–11e). Plastic deformation promotes conglomerate refinement. In this range of loading rates, localized deformation and cracking occur along grain boundaries, curving around groups of grains (Figs. 11a–11c). The average size of a structural element (grain conglomerate) is 80–100 μm.

As shown above, resonant excitation of structural elements of AB2 steel is possible in the impact velocity range 361–381 m/s, resulting in the refinement of large-scale conglomerates. The process of conglomerate refinement is clearly visible in Fig. 12a. When the impact velocity increases to 361–381 m/s, transcrystalline fracture is initiated, with microcracks propagating across grains. Transcrystalline cracks are randomly distributed over the specimen and have a random orientation. This indicates that transcrystalline fracture is initiated by the velocity scatter of mesoparticles, which is quantitatively characterized by the velocity variation. Specimens loaded in the transient and postthreshold regions also contain grain conglomerates. During dynamic deformation, these conglomerates are often highly fragmented. Figure 12b shows such a structure containing transcrystal-

Table 3. Chemical composition of AB2 steel

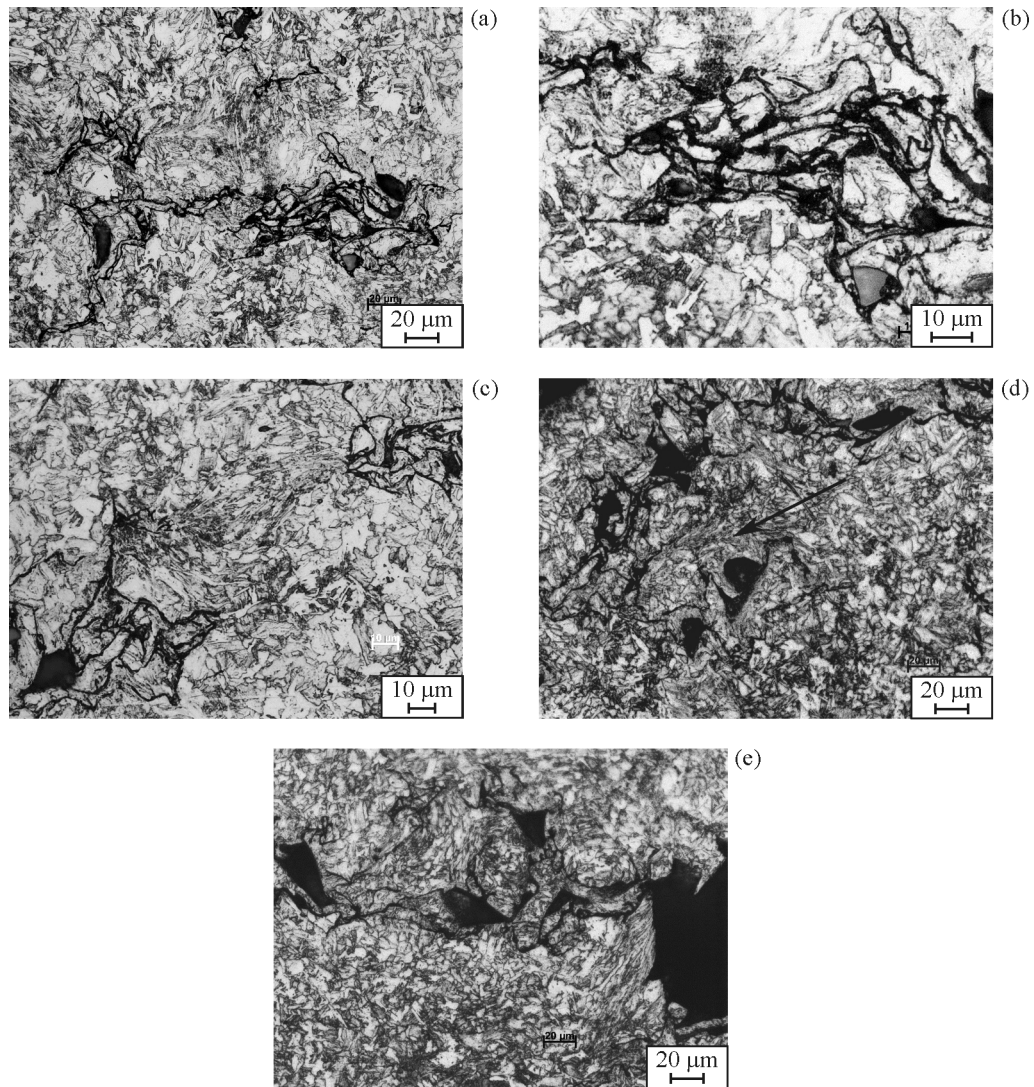| Element	C	Mn	P	S	Cr	Ni	Mo	Si	V	Cu	Fe
AB2	0.1	0.78	0.008	0.35	0.85	3.09	0.21	0.29	0.05	0.60	base

Fig. 11. Fracture morphology of AB2 steel at the prethreshold impact velocity 324 m/s: grain conglomerates (a, b); plastic flow zone (c–e).
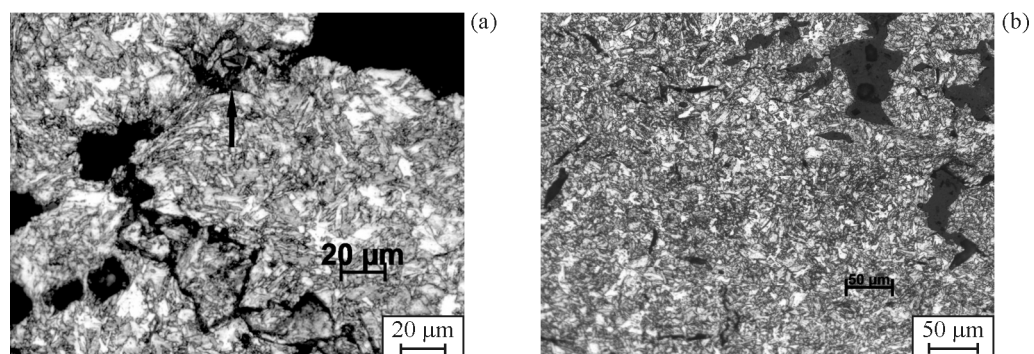

Fig. 12. Fracture morphology of AB2 steel in the transient loading region: 361 (a) and 381 m/s (b).

line cracks with the average size 15 μm and fragmented conglomerates with the average size 50–70 μm, which coincides with the spatial period of plastic flow oscillations calculated by the relaxation model in Sect. 3. The density of transcrystalline microcracks increases with increasing impact velocity (Fig. 13).
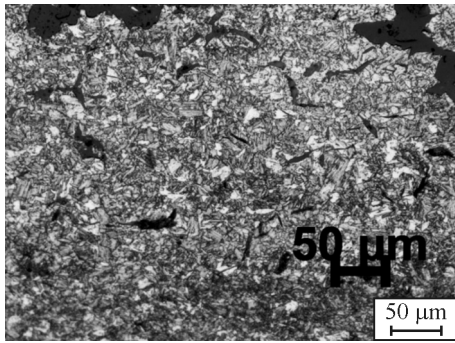
50 μm

Fig. 13. Transcrystalline microcracks in an AB2 steel specimen at the impact velocity 432 m/s.

6. DISCUSSION

The derived results suggest that the change in the mechanism of dynamic fracture of AB2 steels occurs by the following scheme: deformation and fracture along conglomerate boundaries → transcrystalline fracture. Below the impact velocity 361 m/s, the velocity variation is zero, which points to no scatter of particle velocities in this impact velocity range. As the microstructural studies show, at the impact velocity 361 m/s, a part of the large-scale formations is fragmented into small structural formations. This fragmentation is due to the resonant excitation of structural elements, leading to a sharp increase in their velocity spread, i.e. velocity variation. In accordance with expression (5), the higher the rate of change of velocity variation dD/dt, the greater the velocity defect. Thus, the mass velocity defect forms during structural heterogenization of dynamic deformation on the mesoscale. Spatial dispersion of velocity defects is determined by the velocity variation on the meso-1 scale.

Below the strain rate threshold, dynamic fracture occurs by the grain boundary mechanism, when cracks curve around grain conglomerates. When the strain rate threshold is reached, the grain-boundary mechanism is replaced by transcrystalline fracture. Thus, the trigger mechanism responsible for the dynamic fracture mechanism change is the resonant interaction of oscillations of plastic flow and mesoscopic structural elements.

Interferometry of mass velocity reveals local accelerations and decelerations of meso-2 elements of the material. These processes are also manifested in positive and negative values of the velocity defect recorded in local 70–100-μm regions on the free surface of impacted specimens. In other words, the free surface velocity at different points of the target can locally be either lower or higher than the impact velocity. A sharp increase in the particle velocity spread and the appearance of a negative velocity defect on the compression pulse plateau are the second mechanism that triggers the change in the crack formation mechanism, in particular, from grain boundary to transcrystalline fracture. A characteristic feature of transcrystalline fracture is that transcrystalline cracks are randomly oriented and randomly distributed throughout the specimen, without interacting with each other, which increases the dynamic strength of the material.

7. CONCLUSIONS

Since dynamic fracture is always initiated in local regions of the material (the so-called "incipient stage of dynamic fracture"), local recording of impact response, in contrast to integral probing of the entire surface of the target, ensures an identification of specific crack formation mechanisms at the initial fracture stage. This allows determining the direction of structural changes to improve the mechanical characteristics of the material by controlling local characteristics of cracking. Currently, such a method of testing and recording the impact response is an effective way of designing materials with the required mechanical characteristics.

Based on the impact tests, theoretical analysis, and microstructural studies, it was found that that the scale of dynamic deformation and fracture changed by two trigger mechanisms:

(1) resonant excitation of the mesoscopic structure of the material;

(2) a sharp increase in the rate of growth of the mass velocity variation and the appearance of a negative velocity defect.

The moment of transition of the material to a structurally unstable state is determined by the mass velocity variation and velocity defect. These characteristics govern mechanical properties of the material under impact loading. The method proposed for recording these characteristics in real time allows controlling physical mechanisms responsible for the dynamic strength and ductility of the material on the mesoscale.

CONFLICT OF INTEREST

The authors of this work declare that they have no conflicts of interest.

REFERENCES

1. Panin, V.E., Egorushkin, V.E., and Panin, A.V., Physical Mesomechanics of a Deformed Solid as a Multilevel System. I. Physical Fundamentals of the Multilevel Approach, *Phys. Mesomech.*, 2006, vol. 9, no. 3–4, pp. 9–20.

2. Panin, V.E., Egorushkin, V.E., and Elsukova, T.F., Physical Mesomechanics of Grain Boundary Sliding in a Deformable Polycrystal, *Phys. Mesomech.*, 2013, vol. 16, no. 1, pp. 1–8.

3. Makarov, P.V., On the Hierarchical Nature of Deformation and Fracture of Solids and Media, *Phys. Mesomech.*, 2004, vol. 7, no. 3–4, pp. 21–29.

4. *Structural Levels of Plastic Deformation and Fracture*, Panin, V.E. (Ed.), Novosibirsk: Nauka, 1990.

5. Vladimirov, V.I., Nikolaev, V.N., and Priemskii, N.M., Mesoscopic Level of Deformation, in *Physics of Strength and Plasticity*, Zhurkov, S.I. (Ed.), Leningrad: Nauka, 1986, pp. 69–80.

6. Ravichandran, G., Rosakis, A.J., Hodovany, J., and Rosakis, P., On the Convention of Plastic Work into Heat during High-Strain-Rate Deformation, in *AIP Conf. Proc.: Shock Compression of Condensed Matter-2001*, Furnish, M.D., Thadhani, N.N., and Horie, Y-Y., Eds., New York: Melville, 2002, vol. 620, pp. 557–562.

7. Meshcheryakov, Yu.I., *Multiscale Shock Wave Processes in Solids*, St. Petersburg: Nestor-Istoriya, 2018.

8. Barker, L.M., Fine Structure of Compressive and Release Wave Shapes in Aluminum Measured by the Velocity Interferometer Technique, in *Symposium in High Dynamic Pressure*, Paris, 1967, pp. 369–382.

9. Zlatin, N.A., Pugachev, G.S., Volovets, L.D., Zilberbrand, E.L., and Leontyev, S.A., Interferometric Measurement of Parameters of Weak Stress Waves in Solids, *Zh. Tekh. Fiz.*, 1981, vol. 51, no. 7, pp. 1503–1506.

10. Zlatin, N.A., Mochalov, S.M., Pugachev, G.S., and Bragov, A.M., Laser Differential Interferometer, *Zh. Tekh. Fiz.*, 1973, vol. 49, no. 9, pp. 1961–1966.

11. Meshcheryakov, Yu.I. and Prokuratova, E.I., Kinetic Theory of Continuously Distributed Dislocations, *Int. J. Solids Struct.*, 1995, vol. 32, pp. 1711–1726.

12. Prokuratova, E.I. and Indeitzev, D.A., Conditions for the Dislocation Distribution Localization under Dynamic Loading, *Dymat J.*, 1995, vol. I(3/4), pp. 229–233.

13. Yano, K. and Horie, Y.-Y., Discrete Element Modeling of Shock Compression of Polycrystalline Coppe, *Phys. Rev. B*, 1999, vol. 59(21), pp. 13672–13680.

14. Meshcheryakov, Yu.I., Divakov, A.K., Zhigacheva, N.I., Makarevich, I.P., and Barakhtin, B.K., Dynamic Structures in Shock-Loaded Copper, *Phys. Rev. B*, 2008, vol. 78, pp. 64301–64316.

15. Meshcheryakov, Yu.I., *Multiscale Mechanics of Shock Wave Processes*, Singapore: Springer, 2021. http://doi.org/101007/978-981-16-4530-3

16. Duvall, G.E., Propagation of Plane Shock Waves in Stress Relaxing Medium, in *Stress Waves in Inelastic Solids*, Kolsky, H. and Prager, W. (Eds.), Berlin: Springer, 1964, pp. 20–32.

17. Taylor, G.I., The Use of Flat-Ended Projectiles for Determining Dynamic Yield Stress, *Proc. Roy. Soc. Lond. A*, 1948, vol. 194, pp. 289–299.

18. Johnson, J.N. and Barker, L.V., Dislocation Dynamics and Steady Plastic Wave Profiles in 6061-T6 Aluminum, *J. Appl. Phys.*, 1969, no. 10, pp. 4321–4333.

19. Gilman, J.J., Microdynamics of Plastic Flow at Constant Stress, *J. Appl. Phys.*, 1967, vol. 36, no. 9, pp. 2772–2779.

20. Johnson, J.N., Jones, O.N., and Michaels, T.E., Dislocation Dynamics and Single Crystal Constitutive Equation: Shock-Wave Propagation and Precursor Decay, *J. Appl. Phys.*, 1970, vol. 41, no. 6, pp. 2230–2239.

21. Arvidson, T.E., Gupta, Y.M., and Duvall, G.E., Precursor Decay in 1060-Aluminum, *J. Appl. Phys.*, 1975, vol. 46, no. 10, pp. 447–457.

22. Gupta, Y.M. and Duvall, G.E., Dislocation Mechanism for Stress Relaxation in Shocked LiF, *J. Appl. Phys.*, 1975, no. 2, pp. 532–548.

23. Khantuleva, T.A. and Meshcheryakov, Yu.I., Shock-Induced Mesoparticles and Turbulence Occurrence, *Particles*, 2022, no. 5, pp. 407–425. https://doi.org/10.3390/particles5030032

24. Meshcheryakov, Yu.I., Particle Velocity Non-Uniformity and Steady Wave Propagation, *Shock Wave. Detonation. Explosive*, 2016, vol. 26, no. 3. https://doi.org/19.1007/S00193-016-0659-7

25. Indeitzev, D.A., Meshcheryakov, Yu.I., Kuchmin, A.Yu., and Vavilov, D.S., Multiscale Model of Steady-Wave Shock in a Medium with Relaxation, *Acta Mech.*, 2014, vol. 226, no. 3, pp. 917–935. https://doi.org/10.1007/s00707-014-1231-0

26. Cohran, S. and Banner, D., Spall Studies in Uranium, *J. Appl. Phys.*, 1977, vol. 48, no. 7, pp. 2729–2737.